

Shaping Radio Access to Match Variable Wireless Fronthaul Quality in Next-Generation Networks

Marcello Morini¹, Eugenio Moro¹, Ilario Filippini¹, Danilo De Donno², Antonio Capone¹

¹ DEIB, Politecnico di Milano, Milan, Italy - {*name.surname*}@polimi.it

Milan Research Center, Huawei Technologies Italia S.r.l., Milan, Italy - *danilo.dedonno@huawei.com*

Abstract—

The emergence of Centralized RAN (C-RAN) has revolutionized mobile network infrastructure, offering streamlined cell-site engineering and enhanced network management capabilities. As C-RAN gains momentum, the focus shifts to optimizing fronthaul links. While fiber fronthaul guarantees performance, wireless alternatives provide cost efficiency and scalability, making them preferable in densely urbanized areas. However, wireless fronthaul often requires expensive over-dimensioning to overcome the challenging atmospheric attenuation typical of high frequencies. We propose a framework designed to continuously align radio access capacity with fronthaul link quality to overcome this rigidity. By gradually adapting radio access capacity to available fronthaul capacity, the framework ensures smooth degradation rather than complete service loss. Various strategies are proposed, considering factors like functional split and beamforming technology and exploring the tradeoff between adaptation strategy complexity and end-to-end system performance. Numerical evaluations using experimental rain attenuation data illustrate the framework's effectiveness in optimizing radio access capacity under realistically variable fronthaul link quality, ultimately proving the importance of adaptive capacity management in maximizing C-RAN efficiency.

I. INTRODUCTION

Centralized RAN (C-RAN) represents the culmination of the device disaggregation process in Radio Access Networks (RANs). This architecture involves concentrating the baseband (BB) processing of a cluster of cells in a central location and connecting them to Radio Units (RUs) dislocated at the cell sites through high-capacity, low-latency connections, called fronthaul links. This approach has gained significant momentum with the introduction of 5G technologies, which made virtualization techniques more accessible. Recent global market surveys conducted among mobile radio network operators indicate that 80% of the respondents plan to implement C-RAN in at least 20% of their sites (with nearly half of them targeting more than 40% of sites) by the end of 2025, a notable increase from 2022, when the operators aiming for this level of site coverage were 40% [1].

The appeal of C-RAN architecture lies in its ability to streamline cell-site engineering and reduce the geographical distribution of maintenance sites. Centralizing BB processing simplifies the design of RUs in a cost-effective and energy-efficient manner. Moreover, it enhances network coordination and management, enabling better strategies for load balancing, coordinated multi-point communications, cooperative spatial multiplexing, macro-diversity, and mobility management. Additionally, C-RAN facilitates network virtualization, slicing, and openness [2].

The primary technical challenge in C-RAN deployment is designing fronthaul links with sufficient capacity and minimal latency. Two options are available: fiber fronthaul and wireless fronthaul. Fiber fronthaul guarantees high capacity and minimal latency but can be cost-prohibitive due to high trenching expenses, particularly in urban European scenarios [3]. Alternatively, wireless fronthaul provides cost efficiency and allows for rapid, flexible, and scalable deployment, especially in areas where fiber connectivity is impractical or unavailable.

Realizing the full potential of wireless fronthaul relies on establishing high-capacity and reliable links. Commonly utilized technologies for achieving this operate within frequency bands such as D, K, E, V, and W. However, communications at these frequencies are prone to significant propagation losses and are vulnerable to various obstacles and weather conditions. For instance, rainfall can impact the link's power budget, introducing substantial additional attenuation.

Fronthaul and radio access capacities are strongly interdependent. Traditional fronthaul links are engineered to maintain a constant capacity, capable of providing to the RU the highest amount of resources (e.g., Resource Block (RB), MIMO layers) it needs to achieve the maximum data rate in access. However, if fronthaul capacity drops below a certain threshold, the configured access scheme becomes unsustainable and the entire cell drops. Overdimensioning the link budget may be a reasonable solution for wired fronthaul, but it is not efficient nor sustainable for its wireless counterpart.

In response to variable wireless fronthaul link quality, a more effective strategy involves adaptively reducing the required fronthaul rate by gradually degrading end-to-end (E2E) radio access performance. Although temporarily reducing the data rate is preferable to losing a cell entirely, quantifying the impact of access capacity degradation on fronthaul capacity is not straightforward. It hinges on factors like the employed functional split, the cell configuration and the type of beamformer used. Moreover, different radio access throttling countermeasures can be used to mitigate fronthaul link requirements, each with its own advantages and drawbacks depending on the operational scenario. Selecting the optimal scheme is critical to adapt to the available capacity effectively.

This paper introduces a modeling framework designed to align radio access capacity with fronthaul link quality. This framework enables us to estimate the upper bound of radio access capacity achievable with any given fronthaul capacity. Through this, we explore all potential countermeasures to reduce fronthaul link requirements when the highest capac-

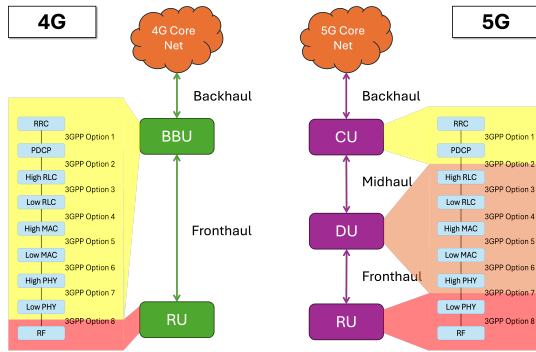


Fig. 1: 3GPP 4G vs 5G RAN architectures and functional split options

ity is unavailable, highlighting their benefits and limitations. Finally, we present numerical examples of variable-quality fronthaul links and their achievable radio access capacity using experimental attenuation time series collected during a rainfall event. These examples demonstrate how radio access capacity throttling can be performed based on available fronthaul capacity.

The rest of the paper is structured as follows. In Sec. II, we discuss C-RAN architectures and components, while in Sec. III we introduce our framework to model fronthaul and radio access capacity. Sec. IV discusses all potential countermeasures for throttling radio access capacity to adapt to the available fronthaul link quality, and numerical examples are given in Sec. V. Finally, Sec. VI concludes the paper.

II. BACKGROUND

In C-RAN, the fronthaul plays a crucial role as the connection layer between a baseband (BB) central unit and a collection of RUs. This design involves the geographic separation and the disaggregation of traditional RAN cell sites into distinct network functions, adhering to a paradigm where RUs, at the far edge of the RAN, primarily handle radio signal reception and transmission at the cell site. Meanwhile, all other functions are centralized within the unit at the opposite endpoint – the proximal endpoint – of the backhaul link.

As depicted in Figure 1, the role of the proximal endpoint has evolved with each generation of mobile communications technology. In 4G RANs, the architecture comprises Base Band Units (BBUs) and RUs interconnected via the fronthaul. In 5G specifications, an additional functional split has been introduced, where real-time signaling procedures are managed by Distributed Units (DUs) connected via midhaul links, while non-real-time higher-layer protocol functions are overseen by the Central Unit (CU).

A more precise delineation of the functions separated by a fronthaul link is provided by 3GPP RAN functional split options, also illustrated in Figure 1. The rationale underlying these options is that the lower the split level, the lesser the signal/data processing is performed at the RU. Consequently, more raw data is transmitted through fronthaul links, resulting in higher throughput.

In today's landscape, Option 7 for fronthaul links stands out as one of the most favored choices for 5G networks, also

supported by the Open RAN (O-RAN) Alliance. This option entails hosting high and low physical (PHY) layer functions at the two endpoints of the fronthaul links. PHY-layer functions are applied to convert transport blocks received from the MAC layer into IQ samples ready for the RF frontend. Within the PHY layer, a more refined functional split can be delineated, allowing for an asymmetric split between uplink and downlink function chains. Two common examples are Option 7-3, which splits the PHY layer between the *scrambling* and the *modulation* functions, thus transporting codewords over the fronthaul link, or Option 7-2, which makes a split between the *precoding* and the *resource element mapping* functions, therefore sending antenna symbols through the fronthaul.

The protocols utilized for the fronthaul interface have evolved over the past decade. Initially, in the early 4G systems, the BBU-RU interface was proprietary to mobile equipment vendors and built upon the Common Public Radio Interface (CPRI) interface, implementing split Option 8. However, in 2017, an updated interface known as Enhanced CPRI (eCPRI) was introduced. The eCPRI interface offers remarkable flexibility and supports multiple split options, all aligned with the 3GPP RAN functional split [4]. Consequently, it quickly emerged as the standard interface linking RU and DU in 5G networks.

Wireless fronthaul capacity issues have been known since C-RAN architectures were first discussed several years ago. Still, we believe that our contributions stand out in several ways from the limited, existing literature. Preliminary fronthaul rate formulas were reported in [5]. That contribution, however, focuses on wired connections and accounts for only a subset of splits. A survey of possible splits and their required rate and latency is provided in [6]. However, the proposed formulae and data are outdated and necessitate a revision. The recent survey in [7] discusses the challenges to be faced when operating a wireless fronthaul, touching on data rate, latency, frame loss, and jitter. Nonetheless, it does not touch on the critical role of the beamforming control information, which may significantly impact the required fronthaul capacity. Also, it lacks a general model for the fronthaul rate calculation. Several ways to answer to wireless fronthaul challenges are mentioned in [8], [9], [10], but without proposing specific methodologies or numerically validating any implementation. Finally, let us point out that our contribution substantially differs from the set of network planning works related to *joint access and fronthaul optimization*, as we propose online reconfiguration strategies that can be easily implemented in greenfield scenarios and already deployed networks.

III. ANALYTICAL MODEL

This section presents a mathematical model of the fronthaul rate for arbitrary cell configuration parameters and different split options of the PHY layer.

Generally speaking, the overall traffic transported by the fronthaul link can be split into 2 components: data directed to the radio access interface to be transmitted by the RU (i.e., unmodulated bits or IQ samples), and antenna beamformer

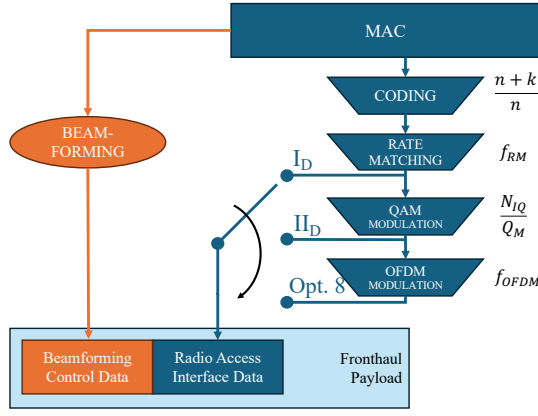


Fig. 2: Downlink physical layer functional blocks impacting the payload

control data directed to the RU's Radio Frequency (RF) chains. The additional data volume required by the synchronization and management planes is not considered in our analysis, as the corresponding volumes are negligible with respect to the overall fronthaul capacity.

The beamforming control rate depends only on the beamforming technology used by the RU and it is independent on the selected split, as shown in Fig. 2.

On the other hand, the radio access interface data is strongly related to the selected split, as this corresponds to the PHY payload size transported on the fronthaul link. Consider Fig. 2 again. On the right side are reported only the downlink PHY functional blocks that modify the size of the payload transported over the fronthaul link and *some* of the most used splits, suggested by [4]. Next to each block of the radio access interface chain, the impact of the performed function on the payload is indicated by means of specific multiplicative factors. Those factors must be sequentially multiplied to the payload dimension when blocks are crossed from the top to the bottom, and divided otherwise. For instance, if *split* I_D is selected, the dimension of the payload coming from the MAC has to be multiplied by the coding factor $\frac{n+k}{n}$, where n is the original size and k are the additional redundancy bits, and the rate matching factor f_{RM} .

While this method can be applied regardless of the direction of access transmission, our analysis focuses on downlink for the sake of simplicity.

A. Radio access interface rate

We now detail the mathematical model that allows us to compute the fronthaul volume contribution given by the radio access interface data. Starting from the bottom part of the right branch in Fig. 2, we consider the time-frequency-space resource grid situated in correspondence of eCPRI *split* II_D (equivalent to 3GPP Option 7-2). Each Resource Element (RE) of each MIMO layer can carry one IQ sample. Considering each IQ sample is encoded by using N_{IQ} bits, and that the symbol transmission time is equal to one OFDM symbol

duration T_S , we obtain the *Split* II_D fronthaul rate formula:

$$R_{FH}^{II_D} = N_{RB} \cdot N_{SC} \cdot N_{MIMO} \cdot N_{IQ} \cdot \frac{1}{T_S}. \quad (1)$$

Here N_{RB} is the number of RBs available for a given channel bandwidth and subcarrier spacing, as defined in [11]. Multiplying this with the number of subcarriers per RB, namely N_{SC} , we obtain the total number of RE. N_{MIMO} is the number of downlink TX antenna ports, corresponding to the maximum number of concurrently active MIMO layers. Note that, although not represented in Fig. 2, this rate equals the fronthaul rate of the uplink *Split* I_U .

To obtain the fronthaul rate of *Split* I_D (equivalent to 3GPP Option 7-3), it suffices to move up by one functional block in Fig. 2 and compute the rate between *QAM modulation* and *Rate matching* blocks. The order- M modulation operation transforms sets of $Q_M = 2^M$ bits in sets of IQ samples, represented with N_{IQ} bits; thus the factor of this block is $\frac{N_{IQ}}{Q_M}$. Dividing the Eq. 1 by such factor, we obtain the following:

$$R_{FH}^{I_D} = N_{RB} \cdot N_{SC} \cdot N_{MIMO} \cdot Q_M \cdot \frac{1}{T_S} \quad (2)$$

Considering splits above the *Rate matching* block is possible but challenging as CRC calculation, channel coding, and rate matching differ for each single physical channel (e.g., PBCH, PDSCH, PDCCH...). Split options below *Split* II_D require to include the OFDM factor f_{OFDM} . The OFDM factor encloses two contributions: one for the frequency-domain zero padding performed over unused REs, and one for the cyclic prefix insertion performed in the time domain.

The total radio access rate the fronthaul link must support depends on the specific Frequency Division Duplexing (FDD) or Time Division Duplexing (TDD) configuration. If the system is TDD, the fronthaul must support the largest access rate between the uplink and the downlink. For the FDD case, the uplink and the downlink channels will have separate RB allocations (resulting in different values of N_{RB}) and potentially different MIMO schemes. In this case, the minimum radio access interface rate corresponds to the sum of the uplink and downlink rates computed according to the equations above.

B. Beamforming control rate

The left branch in Fig. 2 accounts for the main antenna control data generated at the DU-side to be transported over the fronthaul: the beamforming weights. Generally speaking, the beamforming control data varies significantly depending on the beamforming technique in use.

In the case of Analog Beamforming (ABF), the fronthaul link transports N_{ANT} phase-shift coefficient, that is, one per each antenna element. Consequently, the ABF control rate can be computed as follows:

$$R_{FH}^{ABF} = N_{ANT} \cdot b_{PS} \cdot \frac{1}{T_S}, \quad (3)$$

where b_{PS} bits are used to encode the coefficients to be applied at the N_{ANT} antennas every T_S seconds, namely the symbol

time¹. As it will be numerically shown in Sec. V, the resulting rate is significantly lower than the radio access interface rate.

Inversely, Digital Beamforming (DBF) control rate is typically significantly larger. This technology guarantees more accurate antenna radiation patterns by digitally applying amplitude and phase corrections to a large set of signals generated by multiple RF chains. Moreover, different beamforming can be performed across the entire band by applying different weights to every frequency element. However, the increased overall system performance and flexibility come at a higher transport cost. Indeed, the total DBF data rate can be computed as

$$R_{FH}^{DBF} = N_{FE} \cdot N_{MIMO} \cdot N_{RFC} \cdot b_W \cdot \frac{1}{T_S} \quad (4)$$

where N_{FE} is the number of frequency elements that can be controlled (i.e., the control granularity over the frequency resource), N_{RFC} is the number of RF chains, b_W is the bit width of the precoding weights (i.e., the beamforming weights). Here, a reasonable value for N_{FE} may be N_{RB} , while a beamforming switch time of T_S is considered, similarly to the ABF case.

Differently from ABF, the final control data rate can approach the radio access interface rate, thus having a significant impact on the required fronthaul capacity.

Finally, the control rate for Hybrid Beamforming by summing Eqs. 3 and 4 with the proper number of RF chains and antennas.

C. Cell capacity

The formula to compute the radio access capacity of a single RU is provided by 3rd Generation Partnership Project (3GPP) [12]. We report it here with the notation employed in this paper:

$$R_{ACC} = N_{RB} \cdot N_{SC} \cdot N_{MIMO} \cdot Q_M \cdot R_{MAX} \cdot \frac{(1 - OH)}{T_S}. \quad (5)$$

It derives directly from Eq. (2) and includes the value of the target code rate, R_{MAX} , and the overhead due to the control channels, OH , (e.g., PBCH, PRACH). Consequently, it indicates the maximum cumulative effective data rate achievable by the users connected to the antenna. One more factor f_{TDD} should be multiplied in case of TDD adoption, to explicit the portion of resources devoted to uplink and to downlink.

IV. CAPACITY REDUCTION COUNTERMEASURES

Unforeseen channel conditions can reduce the fronthaul link capacity below the threshold required to support the cell. In this case, the communication between the DU and the RU cannot be guaranteed, and the system is considered to be in an outage. However, there exists possible countermeasures to adapt the fronthaul link rate to the instantaneous link capacity variations.

As shown in Sec. III, the required fronthaul rate is a function of the cell configuration and allocated resources.

¹The choice of T_S is technologically challenging for the beamforming hardware, but conservative with respect to the final required fronthaul capacity.

As such, we can act on these to design countermeasures to fronthaul capacity degradation. In this section, we propose two strategies, for which we analyze their advantages and drawbacks and discuss their expected performance. These two strategies will be then applied to real-world measurements of a fronthaul link in Sec. V to numerically evaluate the performance in terms of E2E cell capacity.

A. Cell Reconfiguration (CR)

According to Eq. (1), the fronthaul capacity required to support the radio access interface data rate is directly proportional to the configured cell resources. In particular, this rate increases linearly with the bandwidth and the number of MIMO layers. As such, a straightforward adaptation strategy could consist of an on-the-fly reconfiguration of these cell parameters. For instance, an Frequency Range 2 (FR2) cell working with a bandwidth of 200 MHz could be temporarily reconfigured to use only 100 MHz, yielding a fronthaul rate reduction of a factor 2. A similar effect can be achieved by deactivating MIMO layers.

Concerning the beamforming control data, *cell reconfiguration* does not affect the capacity requirements when ABF is used. On the other hand, the data rate for DBF is once again directly proportional to the bandwidth and number of MIMO layers, as shown in Eq. (4). As such, in the case of hybrid or digital beamforming, the *cell reconfiguration* strategy can effectively reduce the fronthaul traffic by acting on the same parameters.

B. Scheduler-based throttling (SBT)

Cell reconfiguration is a straightforward way of controlling the fronthaul traffic. However, as discussed later in the text, this strategy shows some crucial limitations. For this reason, we propose *scheduler-based throttling* as an alternative adaptation method.

Its rationale is shared with cell reconfiguration, but the factors defining the required fronthaul rate in Eqs. (1) and (4) are controlled at the radio resource management level. Indeed, the resource scheduling process can be instructed to avoid allocating a certain portion of radio resources to reduce the fronthaul capacity requirements.

For instance, if a contiguous portion of RBs is marked as never to be allocated, these do not need to be transported over the fronthaul link. Alternatively, if a subset of MIMO layers is not used to schedule transmissions, the relative fronthaul capacity can be spared. In both cases, the effect is equivalent to a cell reconfiguration, although with increased granularity with respect to the relatively limited set of legal cell parameters.

C. Strategy comparison

While the two strategies detailed above can effectively adapt the fronthaul traffic to the available capacity, they show some differences in complexity and performance.

Cell reconfiguration shows the lowest implementation and execution complexity. Indeed, cell reconfiguration is a natural operation for base stations. *Scheduler-based throttling*, on

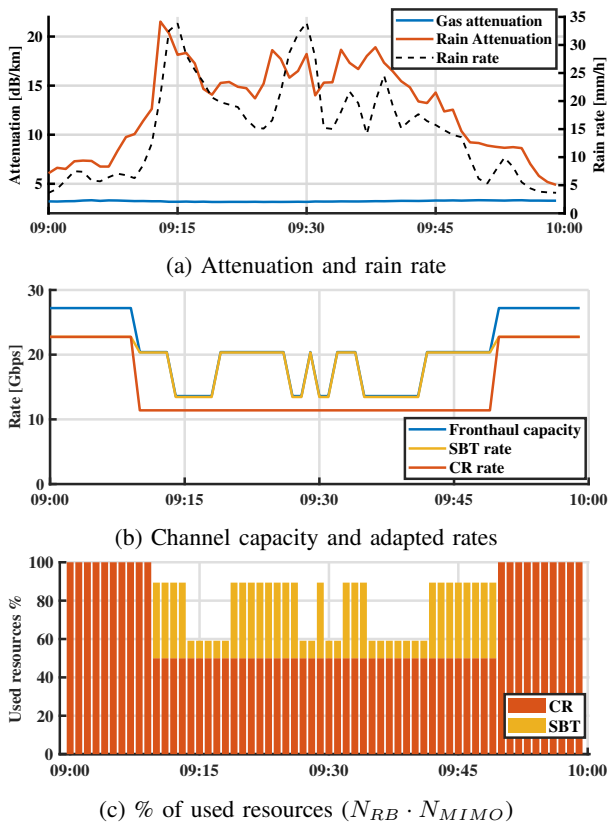


Fig. 3: Time-domain plots of the analyzed scenario

the other hand, requires a custom scheduler that can be controlled based on the instantaneous fronthaul capacity. *Cell reconfiguration* also appears to be compatible with any split, while scheduling control might not be able to throttle the fronthaul traffic for very low splits (e.g., *Split E*) where the baseband signal is exchanged on the fronthaul link.

Nevertheless, the increased complexity of the *scheduler-based throttling* comes with higher adaptation performance. By controlling the scheduling decision, the fronthaul traffic can be throttled with a granularity equivalent to the capacity required to transport a single RB. Consequently, the gap between the fronthaul rate and the available capacity can be reduced to a minimum, resulting in higher access performance.

Cell parameter reconfiguration is generally not designed to be an instantaneous operation that can be carried out frequently. Therefore, the reaction speed of the *cell reconfiguration* approach is limited. Additionally, any reconfiguration might disrupt end-user connectivity, further increasing the cost of applying the strategy. Conversely, scheduling policies can be changed to a Transmission Time Interval (TTI) notice, and they do not cause connectivity disruptions other than the necessary radio access capacity reduction.

V. NUMERICAL ANALYSIS

In this section, we evaluate the impact of the strategies outlined in Sec. IV by applying them to real, measured data as those provided in [13]. We begin by discussing measurements

TABLE I: D-band fronthaul parameters

Distance	1 km
EIRP	65 dBm
RX antenna gain	42 dBi
Free-space path loss	137 dB
Available Fronthaul (FH) modulations	QPSK, 64QAM, 256QAM
Available FH BW	250, 500, 1000, 2000 MHz

and capacity aspects of an experimental wireless link used as a fronthaul candidate. Subsequently, we analyze the results of applying the reconfiguration strategies to this link.

Authors in [13] measure the attenuation over time along a wireless link observed every second for a whole day in the summer of 2023, focusing on both rain and gas (e.g., fog and atmosphere) attenuation. The time series was measured over an E-band link (83 GHz) and then fed into a frequency scaling model to upconvert attenuation measurements to the D-band (156 GHz), more suitable for fronthaul transmissions. A subset of the results are shown in Fig. 3a. The gas attenuation remains relatively constant over the day, at around $3\text{dB}/\text{km}$. The rain attenuation is highly influenced by an intense rain event that happened from 9 to 10 AM, the portion of day shown in the figure. The precipitation rapidly increases up to $34\text{mm}/\text{h}$, therefore classified as a *very heavy rain* event. Such events are not common at the location of the experiment. Indeed, they occur only 0.01% of the time, a small probability that however cannot be neglected to guarantee a five-nines uptime availability.

We use these rain and gas attenuation values to run a model for computing the capacity of a realistic link working at the D-band undergoing the same rain event. The operating parameters of this link are reported in Tab. I. The link transmitter adapts its modulation depending on predefined SINR thresholds detected at a beacon receiver, eventually translating the overall attenuation in up to twelve fronthaul link capacity values. Among them, only three are triggered in the considered dataset: 27.2 Gbps, 20.4 Gbps and 13.6 Gbps. The last two values are experimented only during the measured precipitation event, while the first is seen during the rest of the day. In this work, we assumed that only atmospheric attenuation influences the fronthaul link capacity. However, the discussion can be generalized by considering all other variable parameters in the link budget.

In the next step, we fed the time-varying fronthaul link capacity during the rain event into a simulator implementing both the analytical framework described in Sec. III and the adaptation strategies discussed in Sec. IV. The goal of the simulator is to fill the available fronthaul link *capacity* with the largest fronthaul *rate* possible to provide the largest radio access interface capacity during the rain event. Without loss of generality, the modeled radio access interface considers a millimeter wave (mmWave) RU, implementing up to 200 MHz of bandwidth (i.e., 132 RB), 8 Multiple Input, Multiple Output (MIMO) layers, managed in a TDD fashion, controlled by Analog Beamforming (ABF), and using *Split II_D*. Therefore, the total fronthaul rate is computed as the sum of Eqs. (1)

and (3). In the system we considered, we further assume that $N_{IQ} = 16\text{bits}$, $N_{ANT} = 1024$ and $b_{PS} = 5\text{bits}$, realistic assumptions for a mmWave cell. Fronthaul and ABF rates reach up to 22.7 Gbps and 573 Mbps, respectively.

The link capacity over time and the rate resulting from the countermeasures application are reported in Fig. 3b. We notice that the fronthaul capacity switches to lower modulation orders just after the precipitation starts.

We test the two types of countermeasures. When the *cell reconfiguration* strategy is used, we obtain the behavior reported in orange in Fig. 3b. The system, starting from 200MHz and 8 MIMO layers, halves the bandwidth as the fronthaul capacity is reduced, and keeps this configuration until the end of the rain event. An equivalent effect could be obtained by halving the maximum number of MIMO layers. In case the scheduler can be accessed and programmed (i.e., *scheduler-based throttling*), we get the behavior described in Fig. 3b by the yellow curve, which is almost indistinguishable from the blue one of the link capacity. Varying the radio access capacity at steps of a single RB (which corresponds to 0.76% of the overall capacity), this method has much finer granularity in tuning radio access capacity. Indeed, the yellow curve closely approaches the available fronthaul capacity curve from below.

The improved flexibility of *scheduler-based throttling* is also highlighted with the cumulative bar plot in Fig. 3c, where the percentage of resources used (intended as $N_{RB} \cdot N_{MIMO}$) is reported. As shown, the *Scheduler based throttling* allows us to use up to 87% of the total available resources, instead of the 50% reached by the *Cell reconfiguration*.

The maximum radio access capacity can be computed from Eq. (5), with $R_{MAX} = 948/1024$, $OH = 0.18$ for Downlink (DL) and $f_{TDD}^{DL} = 0.8$. Since it is directly proportional to the fronthaul rate, their trends are equal. Cell downlink access capacity varies from a maximum of 6.9 Gbps to a minimum of 3.4 Gbps in case of Cell reconfiguration, while Scheduler-based Throttling is capable of guaranteeing 6.9 Gbps, 6.0 Gbps and 3.9 Gbps.

Finally, we further illustrate the benefits of applying fronthaul adaptation strategies by comparing it to a more traditional system where no adaptation happens. In the latter case, a conservative choice implies over-provisioning the fronthaul link to guarantee an availability equal to 100%, but at the cost of operating with the minimum reachable rate (i.e., 11.9 Gbps, half of the maximum value). Otherwise, one can set the system to work at the maximum rate but accept 40 minutes of downtime (i.e., 97.2% uptime availability). Both approaches appear to be relatively inefficient when compared to the adaptation techniques. In particular, when *scheduler-based throttling* is applied, it is possible to extract the best rate value in every condition, obtaining 23.3 Gbps for 97.2% of the day, 20.4 Gbps for 1.6% of the day and the minimum capacity of 13.5 Gbps only for the remaining 1.1% of the day. This approach turns the availability value into a step function, meaning that the cell rate is reconfigured according to the available channel capacity such that cumulative availability reaches 100%.

VI. CONCLUSIONS

C-RAN is emerging as a popular architectural solution among mobile radio network operators. Leveraging a wireless fronthaul, C-RAN offers additional flexibility, cost-efficiency, and scalability advantages on top of the benefits of a fiber fronthaul. However, ensuring uninterrupted service necessitates shaping radio access capacity to adapt to the variable channel quality characterizing wireless links.

In this paper, we have presented a comprehensive modeling framework that considers both data and beamformer control information to accurately dimension the required rate on the fronthaul link. We have delved into techniques to adjust access parameters to align with the transport link capacity. Finally, we have validated these techniques using real data obtained from a D-band fronthaul link, demonstrating their efficacy in practical scenarios.

ACKNOWLEDGMENTS

The research in this paper has been carried out in the framework of Huawei-Politecnico di Milano Joint Research Lab. The Authors acknowledge L. Resteghini, F. Capeletti, L. Luini and Huawei Milan research center for the collaboration. The work of E. Moro and I. Filippini was partially supported by the European Union under the Italian National Recovery and Resilience Plan of NextGenerationEU, partnership on “Telecommunications of the Future” (PE00000001 - program “RESTART”, Structural Project 6GWINET).

REFERENCES

- [1] Lightreading.com, “Heavy reading’s operator strategies for 5G transport market leadership survey,” 2021.
- [2] M. Peng, Y. Li, *et al.*, “System architecture and key technologies for 5G heterogeneous cloud radio access networks,” *IEEE Network*, vol. 29, no. 2, pp. 6–14, 2015.
- [3] M. Lashgari, F. Tonini, *et al.*, “Fiber-vs. microwave-based 5G transport: a total cost of ownership analysis,” in *European Conference and Exhibition on Optical Communication*, pp. We1B–5, Optica Publishing Group, 2022.
- [4] Ericsson AB, Huawei Technologies Co. Ltd, NEC Corporation and Nokia, “eCPRI Specification V2.0,” tech. rep., 2019-05-10.
- [5] G. O. Pérez, J. A. Hernández, and D. Larrabeiti, “Fronthaul network modeling and dimensioning meeting ultra-low latency requirements for 5G,” *J. Opt. Commun. Netw.*, vol. 10, pp. 573–581, Jun 2018.
- [6] L. M. P. Larsen, A. Checko, and H. L. Christiansen, “A survey of the functional splits proposed for 5G mobile crosshaul networks,” *IEEE Communications Surveys & Tutorials*, vol. 21, no. 1, pp. 146–172, 2019.
- [7] D. Townend, R. Husbands, *et al.*, “Challenges and opportunities in wireless fronthaul,” *IEEE Access*, vol. 11, pp. 106607–106619, 2023.
- [8] M. Jiang, J. Cezanne, *et al.*, “Wireless fronthaul for 5G and future radio access networks: Challenges and enabling technologies,” *IEEE Wireless Communications*, vol. 29, no. 2, pp. 108–114, 2022.
- [9] M. Peng, C. Wang, *et al.*, “Fronthaul-constrained cloud radio access networks: insights and challenges,” *IEEE Wireless Communications*, vol. 22, no. 2, pp. 152–160, 2015.
- [10] J. Bartelt, P. Rost, D. Wubben, *et al.*, “Fronthaul and backhaul requirements of flexibly centralized radio access networks,” *IEEE Wireless Communications*, vol. 22, no. 5, pp. 105–111, 2015.
- [11] 3GPP, “NR; Base Station (BS) radio transmission and reception,” Technical Specification (TS) 38.104, 3rd Generation Partnership Project (3GPP), 02 2024. Version 17.12.0.
- [12] 3GPP, “NR; User Equipment (UE) radio access capabilities,” Technical Specification (TS) 38.306, 3rd Generation Partnership Project (3GPP), 03 2023. Version 17.4.0.
- [13] E. Verdugo, L. Luini, *et al.*, “Rain attenuation at mmwave and optical bands from visibility and rainfall intensity measurements,” in *EuCAP 2024*, pp. 1-5, 17-22 March 2024, Glasgow, Scotland.